Real time correlation function in a single phase space integral—beyond the linearized semiclassical initial value representation

Jian Liu and William H. Miller

Department of Chemistry and K. S. Pitzer Center for Theoretical Chemistry

University of California,

and Chemical Science Division, Lawrence Berkeley National Laboratory

Berkeley, California 94720-1460

Abstract

It is shown how quantum mechanical time correlation functions [defined, e.g., in Eq. (1.1)] can be expressed, without approximation, in the same form as the linearized approximation of the semiclassical initial value representation (LSC-IVR), or classical Wigner model, for the correlation function [cf. Eq. (2.1)], i.e., as a phase space average (over initial conditions for trajectories) of the Wigner functions corresponding to the two operators. The difference is that the trajectories involved in the LSC-IVR evolve classically, i.e., according to the classical equations of motion, while in the exact theory they evolve according to generalized equations of motion that are derived here. Approximations to the exact equations of motion are then introduced to achieve practical methods that are applicable to complex (i.e., large) molecular systems. Four such methods are proposed in the paper— the full Wigner dynamics (full WD) and the 2nd order WD based on "Winger trajectories", and the full Donoso-Martens dynamics (full DMD) and the 2nd order DMD based on "Donoso-Martens trajectories"—all of which can be viewed as generalizations of the original LSC-IVR method. Numerical tests of these four versions of this new approach are made for two anharmonic model problems, and for each the momentum autocorrelation

function (i.e., operators linear in coordinate or momentum operators) and the force autocorrelation function (non-linear operators) have been calculated. These four new approximate treatments are indeed seen to be significant improvements to the original LSC-IVR approximation.

I. Introduction

Most quantities of interest in the dynamics of complex systems can be expressed in terms of time correlation functions[1]. For example, dipole moment correlation functions are related to absorption spectra, flux correlation functions yield reaction rates, velocity correlation functions can be used to calculate diffusion constants, and vibrational energy relaxation rate constants can be expressed in terms of force correlation functions. The standard real time correlation function is of the form

$$C_{AB}(t) = \mathrm{Tr}\left(\hat{\rho}_0 \hat{A} e^{i\hat{H}t/\hbar} \hat{B} e^{-i\hat{H}t/\hbar}\right) = \tfrac{1}{Z}\mathrm{Tr}\left(e^{-\beta\hat{H}} \hat{A} e^{i\hat{H}t/\hbar} \hat{B} e^{-i\hat{H}t/\hbar}\right) \tag{1.1}$$

or sometimes it is convenient to use the following symmetrized version[2]

$$C_{AB}(t) = \tfrac{1}{Z}\mathrm{Tr}\left(e^{-\beta\hat{H}/2} \hat{A} e^{-\beta\hat{H}/2} e^{i\hat{H}t/\hbar} \hat{B} e^{-i\hat{H}t/\hbar}\right) \tag{1.2}$$

or the Kubo-transformed version[3]

$$C_{AB}^{Kubo}(t) = \tfrac{1}{Z}\int_0^\beta \mathrm{d}\lambda \tfrac{1}{\beta}\mathrm{Tr}\left(e^{-(\beta-\lambda)\hat{H}} \hat{A} e^{-\lambda\hat{H}} e^{i\hat{H}t/\hbar} \hat{B} e^{-i\hat{H}t/\hbar}\right) \tag{1.3}$$

Here $\hat{H}$ is the (time-independent) Hamiltonian for the system, which we assume to be of standard Cartesian form

$$\hat{H} = \frac{\hat{p}^2}{2m} + V\left(\hat{x}\right) \tag{1.4}$$

where we have used 1-dimensional notation for simplicity; m is the mass and $\hat{p}$, $\hat{x}$ are the momentum and coordinate operators, respectively. Also, in Eq (1.1) and (1.2), $Z = \mathrm{Tr}e^{-\beta\hat{H}}$ $\left(\beta = 1/k_B T\right)$ is the partition function, the density operator $\hat{\rho}_0 = e^{-\beta\hat{H}}/Z$ for the system at equilibrium, and $\hat{A}$ and $\hat{B}$ are operators relevant to the specific property of interest. For later use we also define the combination of

operators $\hat{A}$ and the Boltzmann operator, $\hat{A}^{\beta}$, as $\hat{A}^{\beta} = \frac{1}{Z} e^{-\beta \hat{H}} \hat{A}$ for Eq. (1.1), or $\hat{A}^{\beta} = \frac{1}{Z} e^{-\beta \hat{H}/2} \hat{A} e^{-\beta \hat{H}/2}$ for Eq. (1.2), or $\hat{A}^{\beta} = \frac{1}{Z\beta} \int_0^{\beta} \mathrm{d}\lambda e^{-(\beta-\lambda)\hat{H}} \hat{A} e^{-\lambda \hat{H}}$ for the Kubo-transformed case in Eq. (1.3). One of the practical advantages of the time correlation function approach is that the observable of interest can often be obtained from relatively short time information.

For complex (large) systems, there are several ways to approximate the quantum dynamical correlation function such that the result both approaches its classical limit at high temperature and achieves the exact quantum result as $t \to 0$. One such approach is the centroid molecular dynamics (CMD) method of Voth and co-workers[4,5], and another is the ring polymer molecular dynamics (RPMD) method recently proposed by Manolopoulos and co-workers[6]. In these approaches the real time dynamics is related to a modified classical dynamics of the path integral beads of the quantum Boltzmann operator or the centroid of them. For both of these models, the quantum mechanical equilibrium distribution is conserved, i.e., for the case $\hat{A} = 1$, the correlation function is time independent. Also, both of these models give the exact result for harmonic systems if at least one of the operators $\hat{A}$ and $\hat{B}$ is a linear function of position or momentum operators; however, they do not give the correct result if both operators are non-linear operators, even in a harmonic potential [7].

Another class of approaches is based on various initial value representations (IVRs) of semiclassical (SC) theory[8,9]. The SC-IVR provides a way for generating the quantum time evolution operator (propagator) $e^{-i\hat{H}t/\hbar}$ by computing an ensemble of classical trajectories, much as is done in standard classical molecular dynamics (MD) simulations. The simplest, and thus most easily applicable of these approaches include the so-called linearized SC-IVR (LSC-IVR) by the Miller group[10-12]and others[13,14], and the forward-backward semiclassical dynamics (FBSD) approach by the Makri group[15-17]. These methods treat the operator $\hat{A}^{\beta}$ exactly and approximate the Heisenberg time evolution of operator $\hat{B}(t) = e^{i\hat{H}t/\hbar} \hat{B} e^{-i\hat{H}t/\hbar}$ by assuming that the trajectories used to construct the forward and backward propagators, $e^{-i\hat{H}t/\hbar}$ and $e^{i\hat{H}t/\hbar}$, respectively, are infinitesimally close to one another. In the limit of a

harmonic potential, it is straight-forward to show the LSC-IVR gives the exact quantum correlation functions of even nonlinear functions of the position or momentum operator. The accuracy of the correlation function can be systematically improved by the forward-backward IVR (FB-IVR) and a more recent version—the exact forward-backward IVR (EFB-IVR) developed by Miller and co-workers[18], or the initial value series representation proposed by Pollak and co-workers[19]. These more advanced semiclassical methods are able to describe true quantum coherence effects quite well, but they are more difficult to apply because the integrand of the necessary phase space average has a phase cancellation problem that makes Monte Carlo evaluation more difficult. The LSC-IVR and the FBSD methods have the drawback that the distribution generated for the operator $\hat{A}^{\beta}$ is not invariant with time for the case $\hat{A}=1$ (i.e., $\hat{A}^{\beta}=\frac{1}{Z}e^{-\beta\hat{H}}$, the Boltzmann operator itself), though Liu and Makri have demonstrated that this is in fact not much of a problem in practical calculations of auto-correlation functions[17].

The purpose of the paper is to present a novel methodology for calculating real time correlation functions that is more accurate than the LSC-IVR and the FBSD approaches, but still retains their simplicity, i.e., in having no phase cancellation problems in the relevant phase space averages. Section II first shows that it is possible to write the *exact* real time correlation function in a form identical to the original LSC-IVR expression. Section III then develops several practical approximations to these exact expressions, e.g., use of the thermal Gaussian approximation (TGA)[20] for the Boltzmann operator, and also a particular type of 'equilibrium distribution approximation' (EDA). Some numerical implementations of the methodology for the symmetrized force and the standard momentum auto-correlation functions are presented in section IV, including a strongly anharmonic potential and a more challenging quartic model system. Finally, some concluding remarks appear in section V.

II. Exact Dynamics of the Correlation Function

The linearized approximation to the SC-IVR expression for a time correlation function, the LSC-IVR [10-12], leads to the following 'classical Wigner' model for the correlation function

$$C_{AB}(t) = (2\pi\hbar)^{-1} \int dx_0 dp_0 A_w^\beta (x_0, p_0) B_w (x_t, p_t) \tag{2.1}$$

where A_w^β and B_w are the Wigner functions[21] corresponding to these operators,

$$O_w (x, p) = \int d\Delta x \left\langle x - \Delta x/2 \middle| \hat{O} \middle| x + \Delta x/2 \right\rangle e^{ip\Delta x/\hbar} \tag{2.2}$$

for any operator $\hat{O}$. Here (x_0, p_0) is the set of initial conditions (i.e., coordinates and momenta) for a classical trajectory, $(x_t(x_0, p_0), p_t(x_0, p_0))$ being the phase point at time t along that trajectory.

Here we would like to show first that the *exact* expression for a real time correlation can be cast in a form identical to the LSC-IVR in Eq. (2.1), i.e., involving only a single phase space average over the initial conditions for trajectories. This will then provide a solid basis for introducing practical approximations that will be an improvement of the original LSC-IVR method but still maintain its simple structure.

We thus define the operator $\hat{A}^\beta (t) = e^{-i\hat{H}t/\hbar} \hat{A}^\beta e^{i\hat{H}t/\hbar}$ for systems at equilibrium, or more generally $\hat{A}^\beta (t) = e^{-i\hat{H}t/\hbar} \hat{\rho}_0 \hat{A} e^{i\hat{H}t/\hbar}$ for any initial density $\hat{\rho}_0$ of the system, and make use of the well-known identity for the trace of a product of any two operators $\hat{P}$ and $\hat{Q}$,

$$\mathrm{Tr}\left(\hat{P}\hat{Q}\right) = (2\pi\hbar)^{-1} \int dx dp P_w (x, p) Q_w (x, p) \tag{2.3}$$

to express the *exact* real time correlation functions of Eqs. (1.1)-(1.3) as follows

$$C_{AB}(t) = \mathrm{Tr}\left(\hat{A}^\beta (t) \hat{B}\right) = (2\pi\hbar)^{-1} \int dx dp A_w^\beta (x, p; t) B_w (x, p) \tag{2.4}$$

The time evolution of the operator $\hat{A}^\beta (t)$ is governed by the Heisenberg equation of motion,

$$\frac{\partial}{\partial t} \hat{A}^\beta (t) = \frac{i}{\hbar} \left[\hat{A}^\beta (t), \hat{H} \right] \tag{2.5}$$

the Wigner transform of which can be shown to be

$$\frac{\partial}{\partial t} A_w^\beta (x, p; t) = -\frac{p}{m} \frac{\partial A_w^\beta}{\partial x} + \int_{-\infty}^{\infty} J(x, p - \xi) A_w^\beta (x, \xi; t) d\xi \tag{2.6}$$

where

$$J(x,p)=\frac{i}{2\pi\hbar^2}\int_{-\infty}^{\infty}\left[V\left(q+\tfrac{y}{2}\right)-V\left(q-\tfrac{y}{2}\right)\right]e^{-ipy/\hbar}dy \tag{2.7}$$

For a potential for which the derivatives exist, the right-hand side of Eq. (2.6) can be expanded as

$$\frac{\partial}{\partial t}A_w^\beta(x,p;t)=-\frac{p}{m}\frac{\partial A_w^\beta}{\partial x}+V'(x)\frac{\partial A_w^\beta}{\partial p}-\frac{\hbar^2}{24}V^{(3)}(x)\frac{\partial^3 A_w^\beta}{\partial p^3}+\cdots \tag{2.8}$$

Furthermore, if $(x,p)=(x_t,p_t)$ follows some trajectory, i.e., in the Lagrangian picture,

$$\frac{d}{dt}A_w^\beta(x_t,p_t;t)=\frac{\partial A_w^\beta}{\partial x_t}\dot{x}_t+\frac{\partial A_w^\beta}{\partial p_t}\dot{p}_t+\frac{\partial}{\partial t}A_w^\beta(x_t,p_t;t) \tag{2.9}$$

and if the dynamics of the trajectory is chosen to satisfy

$$\frac{d}{dt}A_w^\beta(x_t,p_t;t)=0 \tag{2.10}$$

i.e., the initial value of the distribution function remains invariant along the trajectory, then Eq. (2.8) and Eq. (2.9) imply that the equations of motion of these trajectories are as follows

$$\begin{aligned}\dot{x}_t&=\frac{p_t}{m}\\ \dot{p}_t&=-V'(x_t)+\frac{\hbar^2}{24}V^{(3)}(x_t)\frac{\partial^3 A_w^\beta}{\partial p_t^3}\Big/\frac{\partial A_w^\beta}{\partial p_t}+\cdots=-V'_{eff}(x_t,p_t;t)\end{aligned} \tag{2.11}$$

This new dynamics is similar to classical dynamics except that the classical force is replaced by an effective force $-V'_{eff}$. More discussions about the new dynamics as an analogue to classical dynamics are presented in Appendix A.

The continuity equation,

$$A_w^\beta(x_0,p_0)\,dx_0dp_0=A_w^\beta(x_t,p_t)\,dx_tdp_t \tag{2.12}$$

still applies for this new dynamics, which means that the phase space average in Eq (2.4) can be taken over (x_0,p_0), so that Eq. (2.4) for the *exact* real time correlation function has precisely the same form

as Eq. (2.1) for the LSC-IVR correlation function, except that now $\left(x_t\left(x_0,p_0\right),p_t\left(x_0,p_0\right)\right)$ is the phase point at time t along the trajectory which evolves according to Eq. (2.11).

Interestingly, Eq. (2.8) can be rewritten as

$$-\frac{\partial}{\partial t}A_w^\beta\left(x,p;t\right)=\frac{\partial}{\partial x}\left(A_w^\beta\frac{p}{m}\right)+\frac{\partial}{\partial p}\left[A_w^\beta\left(-V'\left(x\right)+\frac{\hbar^2}{24}V^{(3)}\left(x\right)\frac{1}{A_w^\beta}\frac{\partial^2 A_w^\beta}{\partial p^2}+\cdots\right)\right] \tag{2.13}$$

By making analogy to the classical continuity equation in the form

$$-\frac{\partial\rho}{\partial t}=\nabla\cdot\mathbf{j} \tag{2.14}$$

where $\mathbf{j}=\rho\mathbf{v}$ and $\mathbf{v}=(\dot{x},\dot{p})$, one can generate another version of the dynamics, i.e.,

$$\begin{aligned}\dot{x}_t&=\frac{p_t}{m}\\ \dot{p}_t&=-V'\left(x_t\right)+\frac{\hbar^2}{24}V^{(3)}\left(x_t\right)\frac{1}{A_w^\beta}\frac{\partial^2 A_w^\beta}{\partial p_t^2}+\cdots=-V'_{eff}\left(x_t,p_t;t\right)\end{aligned} \tag{2.15}$$

Although the equations of motion governed by Eq. (2.15) do not satisfy Eq. (2.10) and Eq. (A.1), this kind of dynamics has its own merit as we shall see below. Since the continuity equation Eq. (2.12) always holds, the exact real time correlation function also has the same form as Eq. (2.1), the original LSC-IVR method, with the trajectory now evolving according to Eq. (2.15).

The exact quantum correlation function thus has the same form as the LSC-IVR approximation in Eq. (2.1), both being given by a single phase space over the initial conditions for trajectories. The only difference is the evolution of the trajectories: in the LSC-IVR they are governed by classical mechanics, while that in the exact case they are governed by the dynamics specified by Eq. (2.11) or (2.15). As is clear from Eq. (2.11) or (2.15), the original LSC-IVR method can be viewed as the limit of the exact correlation function as $\hbar\to 0$, or the limit of a harmonic potential. In other words, the exact dynamics that of Eq. (2.11) or (2.15) enables us to improve the real time dynamics in the LSC-IVR method.

When $\hat{A}=1$ or $\hat{A}^\beta\left(t\right)=e^{-i\hat{H}t/\hbar}\hat{\rho}_0 e^{i\hat{H}t/\hbar}=\hat{\rho}\left(t\right)$, Eq. (2.6) and (2.8) reduce to the conventional equations of motion for the Wigner distribution function of the density operator[21,22], and trajectories

governed by Eq. (2.11) become "Wigner trajectories"[23] in the literature, and those governed by Eq. (2.15) become what we term here Donoso-Martens (DM) trajectories[24]. Since in practice the equations of motion described by Eq. (2.11) or (2.15) are usually truncated at order of $\hbar^2$, DM trajectories obey Ehrenfest's theorem $\langle \dot{p} \rangle = \mathrm{Tr}\left(\dot{p}\hat{\rho}(t) \right) = -\langle V'(\hat{x}) \rangle$, so that the average energy $\langle E \rangle = \mathrm{Tr}\left(\hat{H}\hat{\rho}(t) \right)$ is invariant with time[24], but Wigner trajectories do not have this desirable property.

III. Equilibrium Distribution Approximations

Though we have expressed the exact quantum time correlation function in the same form as the LSC-IVR approximation, Eq. (2.1), the dynamics (i.e., the trajectories) which go into it are now determined by Eq. (2.11) or (2.15), rather than by the classical equations of motion. To evaluate the effective force $-V'_{eff}$ that determines these trajectories, however, requires that the function $A_w^\beta(x_t, p_t; t)$ be known. Furthermore, Eq. (2.11) or (2.15) requires many (in fact, generally an infinite number of) terms containing derivatives of the potential and those of $A_w^\beta(x_t, p_t; t)$ (though the truncation of the effective force $-V'_{eff}$ at order $\hbar^2$ may sometimes be a good approximation). The direct calculation of $A_w^\beta(x_t, p_t; t)$ via Eq. (2.8) requires the propagation of an ensemble of trajectories of the system which are entangled through the effective force $-V'_{eff}$, making the approach unfeasible for anharmonic systems with many degrees of freedom. A better strategy, an analog of the approach proposed by Liu and Makri[25] in Bohmian dynamics, is to make the trajectories independent of one another by using their stability properties to update $A_w^\beta(x_t, p_t; t)$ and its derivatives along the trajectory, thus making it possible for Monte Carlo (MC) simulations of higher dimensional systems. Such an approach, however, is still probably not feasible for condensed phase systems.

For systems at equilibrium, when $\hat{A} = 1$ the operator $\hat{A}^\beta(t) = \hat{\rho}(t) = \frac{1}{Z} e^{-\beta\hat{H}} = \hat{\rho}(0)$ is time-independent, which means that the Wigner transform of the density operator and its derivatives are time invariant, i.e.,

$$\rho_w(x,p;t)=\rho_w(x,p;0)\equiv\rho_w^0(x,p) \tag{3.1}$$

and

$$\begin{aligned}\frac{\partial}{\partial x}\rho_w(x,p;t)&=\frac{\partial}{\partial x}\rho_w(x,p;0)\equiv\frac{\partial}{\partial x}\rho_w^0(x,p)\\ \frac{\partial}{\partial p}\rho_w(x,p;t)&=\frac{\partial}{\partial p}\rho_w(x,p;0)\equiv\frac{\partial}{\partial p}\rho_w^0(x,p)\end{aligned} \tag{3.2}$$

and so on. Motivated by this observation, we introduce the 'equilibrium distribution approximation' (EDA) as follows: for any operator $\hat{A}$, we approximate the *ratios* of the quantities in Eqs. (2.11) and (2.15) by what they would be with $\hat{A}=1$, i.e.,

$$\frac{\partial^3 A_w^\beta}{\partial p_t^3}\Big/\frac{\partial A_w^\beta}{\partial p_t}\approx\lim_{\hat{A}\to 1}\frac{\partial^3 A_w^\beta}{\partial p_t^3}\Big/\frac{\partial A_w^\beta}{\partial p_t}=\frac{\partial^3\rho_w^0(x_t,p_t)}{\partial p_t^3}\Big/\frac{\partial\rho_w^0(x_t,p_t)}{\partial p_t} \tag{3.3}$$

and so on in the equations of motion in Eq. (2.11), and

$$\frac{1}{A_w^\beta}\frac{\partial^2 A_w^\beta}{\partial p_t^2}\approx\lim_{\hat{A}\to 1}\frac{1}{A_w^\beta}\frac{\partial^2 A_w^\beta}{\partial p_t^2}=\frac{1}{\rho_w^0(x_t,p_t)}\frac{\partial^2\rho_w^0(x_t,p_t)}{\partial p_t^2} \tag{3.4}$$

and so on in the equations of motion in Eq. (2.15). This leads to great simplification in the practical aspects of integrating the generalized equations of motion, as will be seen below, and will also be seen to be correct in various limits.

If the effective force $-V'_{eff}$ in Eq. (2.11) is truncated at the order of $\hbar^2$, then the equations of motion become

$$\begin{aligned}\dot{x}_t&=\frac{p_t}{m}\\ \dot{p}_t&=-V'_{eff}(x_t,p_t;t)=-V'(x_t)+\frac{\hbar^2}{24}V^{(3)}(x_t)\frac{\partial^3\rho_w^0(x_t,p_t)}{\partial p_t^3}\Big/\frac{\partial\rho_w^0(x_t,p_t)}{\partial p_t}\end{aligned} \tag{3.5}$$

which we term '2nd order Wigner dynamics' (2nd order WD). Similarly the truncation of the effective force $-V'_{eff}$ in Eq. (2.15) at the order of $\hbar^2$ leads to

$$\begin{aligned}\dot{x}_t &= \frac{p_t}{m} \\ \dot{p}_t &= -V'_{eff}\left(x_t, p_t; t\right) = -V'\left(x_t\right) + \frac{\hbar^2}{24} V^{(3)}\left(x_t\right) \frac{1}{\rho_w^0\left(x_t, p_t\right)} \frac{\partial^2 \rho_w^0\left(x_t, p_t\right)}{\partial p_t^2}\end{aligned} \tag{3.6}$$

which is termed '2nd order Donoso-Martens dynamics' (2nd order DMD). Both the 2nd order WD and the 2nd order DMD can be viewed as a lowest order perturbation correction to classical dynamics by adding quantum effects to order $\hbar^2$.

Quite remarkably, however, the EDA enables us to include *all higher orders* of $\hbar^2$ into the effective force $-V'_{eff}$. Notice that the left-hand side of Eq. (2.8) or (2.13) goes to zero in the limit $\hat{A} \to 1$, so that the equations of motion in Eq. (2.11) with the EDA become

$$\begin{aligned}\dot{x}_t &= \frac{p_t}{m} \\ \dot{p}_t &= -V'_{eff}\left(x_t, p_t; t\right) = -\frac{p_t}{m} \frac{\partial \rho_w^0\left(x_t, p_t\right)}{\partial x_t} \Big/ \frac{\partial \rho_w^0\left(x_t, p_t\right)}{\partial p_t}\end{aligned} \tag{3.7}$$

which we term 'full Wigner dynamics' (full WD), and those in Eq. (2.13) with the EDA lead to

$$\begin{aligned}\dot{x}_t &= \frac{p_t}{m} \\ \dot{p}_t &= -V'_{eff}\left(x_t, p_t; t\right) = -\frac{1}{\rho_w^0\left(x_t, p_t\right)} \int \frac{p_t}{m} \frac{\partial \rho_w^0\left(x_t, p_t\right)}{\partial x_t} dp_t\end{aligned} \tag{3.8}$$

which we refer to as 'full Donoso-Martens dynamics' (full DMD). Here the integral is an indefinite integral, which can be integrated analytically with the approximations to $\rho_w^0\left(x_t, p_t\right)$ that we describe in next section.

In the high temperature limit, $\beta \to 0$, the Wigner transform of the equilibrium density operator reduces to the classical Boltzmann distribution, i.e.,

$$\rho_w^0\left(x, p\right) \to \tfrac{1}{Z} \exp\left[-\beta\left(\frac{p^2}{2m} + V\left(x\right)\right)\right] \tag{3.9}$$

and in this limit it is straight-forward to verify that all the proposed equations of motion in Eq. (3.5), (3.6) , (3.7) or (3.8) reduce to classical mechanics. Also, in the limit of a harmonic potential, when $V^{(3)}\left(x\right)$

and higher derivatives vanish, these proposed equations of motions are exact. Hence the real time correlation function in Eq. (2.1), with the generalized equations of motion in Eq. (3.5), (3.6), (3.7) or (3.8) , is exact in three important limits (as is the original LSC-IVR method): (i) the classical (or high-temperature) limit, (ii) the limit of a harmonic potential, and (iii) the short-time limit $t \to 0$. What is more important, however, is that they are expected to give a better approximation to the correlation for longer time than the original LSC-IVR method. These four proposed methods can thus be thought of as *improved* LSC-IVR methods, since they have the same form as Eq. (2.1), differing only in the equations of motion which generate the trajectories. The full WD and the full DMD methods, in particular conserve the distribution generated for the operator $\hat{A}^{\beta}$ for the case $\hat{A} = 1$, which the original LSC-IVR method fails to do.

IV. Thermal Gaussian approximation

Calculation of the Wigner function for operator $\hat{B}$ in Eq. (2.1) is usually straight-forward; in fact, $\hat{B}$ is often a function only of coordinates or only of momenta, in which case its Wigner function is simply the classical function itself. Calculating the Wigner function $A_w^{\beta}(x_0, p_0)$ or $\rho_w^0(x_t, p_t)$, however, involves the Boltzmann operator with the total Hamiltonian of the complete system, so that carrying out the multidimensional Fourier transform to obtain it is far from trivial. Furthermore, it is necessary to do this in order to obtain the distribution of initial conditions of momenta p_0 for the real time trajectories. A rigorous way to treat the Boltzman operator is via a Feynman path integral expansion, but it is then in general not possible to evaluate the multidimensional Fourier transform explicitly to obtain the Wigner function $A_w^{\beta}(x_0, p_0)$ or $\rho_w^0(x_0, p_0)$, as discussed by Liu and Miller[12]. The inability to calculate the Wigner function of $\hat{A}^{\beta}$ exactly is in fact the reason for the various harmonic and local harmonic approximations to the Boltzmann operator[10,12,14]. These approximations have been successfully applied to some complex systems[12,26].

With such approximations for the Boltzmann operator, all four approximate methods proposed in section III for the real time dynamics can readily applied. Here we use the thermal Gaussian approximation[20] (TGA) that we have implemented into the LSC-IVR calculation recently[12]. In the TGA, the Boltzmann matrix element is approximated by a Gaussian form:

$$\left\langle x\left|e^{-\tau\hat{H}}\right|q_0\right\rangle=\left(\frac{1}{2\pi}\right)^{3N/2}\frac{1}{\left|\det\left(G(\tau)\right)\right|^{1/2}}\exp\left(-\frac{1}{2}\left(x-q(\tau)\right)^{T}G^{-1}(\tau)\left(x-q(\tau)\right)+\gamma(\tau)\right) \tag{4.1}$$

where $G(\tau)$ is an imaginary-time dependent real symmetric and positive-definite matrix, $q(\tau)$ the center of the Gaussian, and $\gamma(\tau)$ a real scalar function. The parameters are governed by the equations of motion:

$$\begin{aligned}
&\frac{d}{d\tau}G(\tau)=-G(\tau)\left\langle\nabla\nabla^{T}V\left(q(\tau)\right)\right\rangle G(\tau)+\hbar^{2}m^{-1}\\
&\frac{d}{d\tau}q(\tau)=-G(\tau)\left\langle\nabla V\left(q(\tau)\right)\right\rangle\\
&\frac{d}{d\tau}\gamma(\tau)=-\frac{1}{4}Tr\left(\left\langle\nabla\nabla^{T}V\left(q(\tau)\right)\right\rangle G(\tau)\right)-\left\langle V\left(q(\tau)\right)\right\rangle
\end{aligned} \tag{4.2}$$

with the notation

$$\left\langle h(q)\right\rangle=\left(\frac{1}{\pi}\right)^{3N/2}\frac{1}{\left|\det\left(G(\tau)\right)\right|^{1/2}}\int_{-\infty}^{\infty}dx\left(-\left(x-q(\tau)\right)^{T}G^{-1}(\tau)\left(x-q(\tau)\right)\right)h(x) \tag{4.3}$$

The initial conditions for the imaginary time propagation are

$$q(\tau\simeq 0)=q_0;\ G(\tau\simeq 0)=\hbar^{2}\tau m^{-1};\ \gamma(\tau\simeq 0)=-\tau V(q_0) \tag{4.4}$$

The Wigner function $A_w^{\beta}(x_0,p_0)$ with the TGA can then be expressed as follows

$$
\begin{aligned}
A_w^\beta\left(x_0,p_0\right) = \frac{1}{Z}\int dq_0 \, & \frac{1}{(4\pi)^{3N/2}} \frac{\exp\left(2\gamma\left(\frac{\beta}{2}\right)\right)}{\left|\det G\left(\frac{\beta}{2}\right)\right|^{1/2}} \\
& \cdot \frac{1}{\pi^{3N/2}\left|\det G\left(\frac{\beta}{2}\right)\right|^{1/2}} \exp\left(-\left(x_0 - q\left(\frac{\beta}{2}\right)\right)^T G^{-1}\left(\frac{\beta}{2}\right)\left(x_0 - q\left(\frac{\beta}{2}\right)\right)\right) \\
& \cdot \frac{\left|\det G\left(\frac{\beta}{2}\right)\right|^{1/2}}{\left(\pi\hbar^2\right)^{3N/2}} \exp\left(-p_0^T G\left(\frac{\beta}{2}\right) p_0 / \hbar^2\right) \\
& \cdot f_{A^\beta}^{TGA}\left(x_0, p_0, q\left(\frac{\beta}{2}\right)\right)
\end{aligned}
\tag{4.5}
$$

where

$$
f_{A^\beta}^{TGA}\left(x_0, p_0, q\left(\frac{\beta}{2}\right)\right) = A\left(q_0\right) \tag{4.6}
$$

for local operators with $\hat{A}^\beta = e^{-\beta\hat{H}/2} A\left(\hat{x}\right) e^{-\beta\hat{H}/2}$ (notice $\rho_w^0\left(x,p\right) = A_w^\beta\left(x,p\right)$ for $\hat{A}=1$), and

$$
f_{A^\beta}^{TGA}\left(x_0, p_0, q\left(\frac{\beta}{2}\right)\right) = p_0 - i\hbar G^{-1}\left(\frac{\beta}{2}\right)\left(x_0 - q\left(\frac{\beta}{2}\right)\right) \tag{4.7}
$$

for the momentum operator $\hat{A} = \hat{p}$ with $\hat{A}^\beta = e^{-\beta\hat{H}}\hat{p}$, etc.

The TGA enables one to calculate the effective force $-V_{eff}'$ explicitly in the equations of motion for the four methods described in Section III, and hence real time correlation functions based on Eq. (2.1).

V. Example calculations

In order to test how well the four types of generalized dynamics described in Section III perform within the framework of Eq. (2.1), we have carried out calculations for two 1-dimensional models, at a high temperature $\beta = 1$ and a low temperature $\beta = 8$, comparing the results to the classical, the original LSC-IVR, and the exact quantum results. The symmetrized force autocorrelation (a nonlinear local operator) and the standard momentum autocorrelation function are calculated at both temperatures to investigate how well the EDA performs for different operators $\hat{A}$ and for the four different versions of the dynamics.

(a) Anharmonic oscillator

The first model we consider is an asymmetric anharmonic oscillator

$$V(x) = \tfrac{1}{2} m\omega^2 x^2 - 0.10x^3 + 0.10x^4 \tag{5.1}$$

with $m = 1$, $\omega = \sqrt{2}$ and $\hbar = 1$. This quite anharmonic potential has been used as a test and discussed previously with the LSC-IVR and the FBSD methods[12,15,27]. Results for the force autocorrelation functions are shown at two different temperatures in Figs. 1 and 3, while those of the momentum autocorrelation functions are shown in Figs. 2 and 4. At both temperatures, we use 21 imaginary trajectories (to generate the Boltzmann operator via the TGA) with the imaginary time step of 0.1, and a large number of real time trajectories generated from each imaginary trajectories with a real time step of 0.02. The velocity Verlet integrator was used for both real and imaginary time dynamics.

Consider first the higher temperature case ($\beta = 1$), Figs. 1 and 2, for the force-force and momentum-momentum autocorrelation functions, respectively. Even at this temperature, however, the classical results still deviate somewhat from the quantum results with regard to both the initial value at $t = 0$ and the dephasing for longer times. The LSC-IVR method and various improved versions proposed in section III are able to describe the correct result for approximately the first two vibrational periods ($t < 10$). The original LSC-IVR method dephases more rapidly than the quantum result due to coherence effects. The full WD and the full DMD methods dephase the least, but there is a noticeable frequency shift at long times (after three vibrational periods). The 2nd WD method is even worse regarding the frequency shift but the 2nd DMD method seems to correct this error. In the very high-temperature regime ($\beta = 0.1$), the correlation function calculated by all methods and the exact quantum correlation function approach the classical result (figures not shown here), as discussed in section IV.

Results for the much lower temperature ($\beta = 8$) are shown in Figs. 3 and 4, and here the classical results depart from quantum results with regard to both amplitude of the oscillation (drastically) and frequency (noticeably). The original LSC-IVR method provides a good description for the first vibrational period and is semi-quantitative over several more periods. The 2nd DMD method improves the results systematically in both amplitude of the oscillation and frequency for longer times over the original LSC-IVR results, while 2nd WD method does similarly for the amplitude of the oscillation but with a noticeable

frequency shift. The full WD and full DMD methods match the exact quantum result almost perfectly except for a slight frequency shift after quite long time ($t > 25$).

It can be seen that the EDA behaves similarly for both the symmetrized momentum and the force autocorrelation functions despite the fact that the operators are linear in the former case and non-linear in the latter, and the difference between the standard and the symmetrized correlation functions.

(b) Quartic potential

The next model potential studied is the following pure quartic potential

$$V(x) = 0.25x^4 \tag{5.2}$$

with $m = 1$ and $\hbar = 1$. This is a more challenging case since no harmonic term is involved and hence represents a severe test whether the various approximate methods proposed in section III can describe the purely quantum coherent collisions of a broad thermal wave packet against the quartic potential wall. This model has been studied by the CMD and the RPMD dynamics only for the position auto-correlation function[5,6].

The results for the symmetrized force (a very nonlinear operator) autocorrelation functions are shown at two different temperatures in Figs. 5 and 7, while those of the momentum autocorrelation functions are shown in Figs. 6 and 8. The simulation details for this model are the same as those for the previous potential.

Figs. 5 and 6 show that at the temperature $\beta = 1$ the classical result fails to describe the long-time oscillations in the exact quantum results; the LSC-IVR method does little to correct this, and neither do the four new methods that we test in this paper. We expect that the truncated methods (2^{nd} order WD and 2^{nd} order DMD methods) are not able to capture quantum coherences because "quantum coherences are reflected in the Winger function as 'sub-Planckian' oscillations" [28] and any lower order truncations of the propagation of the Winger function fail to describe such effects[29]. The failures of the full WD and the full DMD methods indicate that the EDA that we introduced in section III, i.e., Eq. (3.3), is not capable of describing quantum coherence of the real time correlation function. However, in many cases for complex

systems in the condensed matter phase, such long time coherence effects shown in one-dimensional models are expected to be quenched by coupling among the various degrees of freedom[9,30], and most important is the short time dephasing behavior which can be accurately described by the various methods in this paper.

At the much lower temperature ($\beta = 8$) in Figs. 7 and 8, the classical results depart drastically from quantum results with regard to both the amplitude of the oscillation and the frequency even from the very beginning. The original LSC-IVR method provides reasonably good results for the first vibrational period, but dephases too quickly afterwards and completely vanishes after almost two periods. The 2nd order DMD method is a significant improvement over the original LSC-IVR method in amplitude of the oscillation and reproduces the frequency best, although there is still dephasing. The 2nd order WD method improves the amplitude of the oscillation but generates a pronounced frequency shift. The full WD and full DMD methods behave similarly, giving the amplitude of oscillation quite well (the small remaining error being due to error generated by the TGA treatment) and with slightly more frequency shift than the 2nd order DMD method.

The better behavior at the low temperature is understandable: quantum statistical effects in the correlation functions show their importance for longer time (as the thermal time $\hbar\beta$ is longer) and the EDA also reflects that in the equations of motion of the various methods listed in section III. It is clearly demonstrated that in both the anharmonic model and the quartic potential, the full WD, the full DMD, and the 2nd order DMD methods improve the original LSC-IVR method to (much) longer times at low temperatures.

The 2nd order DMD method works systematically better in all cases than the 2nd order WD method. This is because of the merit of the 2nd order DMD method that is mentioned before, i.e., that the ensemble of all DM trajectories obey Ehrenfest's theorem, which is not true for the 2nd order WD method.

Again, we notice that the EDA behaves similarly for both the symmetrized force and momentum autocorrelation functions; i.e., how the EDA performs seems to be independent of the operator $\hat{A}$ and the version of the real time correlation function. Notice that the force operator is very nonlinear.

VI. Concluding remarks

In this paper we have first shown that the *exact* time correlation function [Eqs. (1.1)-(1.3)] can be written in the form of the LSC-IVR/classical Wigner approximation given by Eq. (2.1), i.e., as a phase space average over initial conditions for trajectories, with the Wigner function for Boltzmannized operator, $\hat{A}^{\beta}$, evaluated at the initial phase point and that for operator $\hat{B}$ evaluated at the time evolved phase point. The difference is that for the LSC-IVR the dynamics (i.e., the time evolution of the trajectories) is that given by the classical equations of motion, while the trajectories in the exact theory are determined by generalized equations of motion. This exact formulation serves as a basis for making approximations to obtain practical methods for application to real molecular systems.

For systems at equilibrium, the EDA provides a feasible and reasonably good approximation. In these examples it is seen to perform similarly for different versions of the autocorrelation function and for different operators $\hat{A}$. Four approximate methods based on the EDA were proposed and tested—the full WD, the full DMD, the 2nd order WD and the 2nd order DMD methods—which can all be viewed as improvements to the original LSC-IVR approximation. The overall results can be summarized as follows. All four methods account for appreciable quantum effects in the correlation functions for short times, for all temperatures, as does the original LSC-IVR. The full WD, the full DMD, the 2nd order DMD methods are good for (much) longer time in low temperature regime than the original LSC-IVR. The 2nd order WD method gives a better description of dephasing effects than the original LSC-IVR method, but it also causes a pronounced frequency shift in the correlation function and is not as good as the former three proposed methods; we attribute this behavior to the fact that it does not obey Ehrenfest's theorem.

Combined with the TGA or other harmonic or local harmonic approximations for the Boltzmann operator, all four methods proposed here can be applied to condensed phase systems in realistic situations, since they do not involve oscillatory factors in the necessary phase space averages. Work is in progress to see how much these new methods improve the LSC-IVR for realistic molecular systems. It will also be interesting in future work to see if one can construct a better approximation than the EDA, e.g., by taking account of operator $\hat{A}$ (rather than taking the limit $\hat{A} \to 1$) in Eq. (3.3) or (3.4).

Finally, we note that though the Wigner transformation was used as the starting point in this paper [Eq. (2.4)], the methodology can in principle be generalized to any quantum phase space transformation, such as the Husimi distribution function[31] , or the Glauber-Sudarshan P and Q functions[32], etc.

Acknowledgement

This work was supported by the Office of Naval Research Grant No. N00014-05-1-0457 and by the National Science Foundation Grant No. CHE-0345280.

Appendix A

In light of Eqs. (2.10) and (2.12), one sees that the volume element in phase space is invariant, i.e., the volume of infinitesimal phase space obeys

$$dx_0 dp_0 = dx_t dp_t \tag{A.1}$$

Eqs. (2.10) and (A.1) reveal the dynamics governed by Eq. (2.11) is an analogue to classical dynamics. An interesting and perhaps useful derivation based on this is that the ensemble average can be replaced by the time average as long as the system is assumed to be ergodic.

To show this, we first define the ensemble average of some physical property $B(x,p)$ on the probability surface $\delta\left(\mathscr{P}(x,p)=\mathscr{P}_0\right)$ as

$$\langle B\rangle_{ens} = \frac{1}{\Sigma\left(\mathscr{P}_0\right)}\int dxdpB(x,p)\delta\left(\mathscr{P}(x,p)=\mathscr{P}_0\right) \tag{A.2}$$

where $\Sigma\left(\mathscr{P}_0\right)$ is the area of the surface, i.e,

$$\Sigma\left(\mathscr{P}_0\right) = \int dxdp\delta\left(\mathscr{P}(x,p)=\mathscr{P}_0\right) \tag{A.3}$$

Eq. (A.2) is in fact a generalized definition from classical dynamics: in classical mechanics, the probability distribution is actually a function of energy $\mathscr{P}(x,p)=\mathscr{P}\left(E=H(x,p)\right)$, the probability surface $\delta\left(\mathscr{P}(x,p)=\mathscr{P}_0\right)$ coincide with the energy surface $\delta\left(H(x,p)=E_0\right)$ and the ensemble average on the probability surface $\delta\left(\mathscr{P}(x,p)=\mathscr{P}_0\right)$ is just the microcanonical ensemble. Any trajectory has to be on some probability surface as long as the dynamics satisfies Eq. (2.10), i.e., here,

$$\frac{d}{dt}\mathscr{P}(x_t,p_t;t)=0 \tag{A.4}$$

We then define the time average of the physical property $B(x,p)$ along some trajectory as

$$\langle B\rangle_T = \lim_{T\to\infty}\frac{1}{T}\int_{t_0}^{t_0+T} B(x_t,p_t)dt \tag{A.5}$$

If the ergodicity holds in the system, the ensemble average on the probability surface equals to the time average along some trajectory on that probability surface, i.e.,

$$\langle B \rangle_{ens} = \langle B \rangle_{T} \tag{A.6}$$

which is a familiar argument for the molecular dynamics (MD) community.

Thus, the analogues of the new dynamics presented in Eq. (2.11) to classical dynamics listed in Eqs. (2.10) and discussed in this appendix opens the gate to introduce some techniques similar to those of the conventional MD simulation into the calculation of the *exact* formulation of the real time correlation function Eq. (2.1) associated with Eq. (2.11). For example, for the canonical ensemble, one might replace the phase space integral in Eq. (2.1) by a time average, if the dynamics in Eq. (2.11) is modified in a similar way in which classical dynamics is modified in the Anderson thermostat[33] or the Nosé-Hoover thermostat[34] to describe the classical Boltzmann distribution.

References

[1] B. J. Berne and G. D. Harp, Adv. Chem. Phys. **17**, 63 (1970).

[2] W. H. Miller, S. D. Schwartz, and J. W. Tromp, Journal of Chemical Physics **79** (10), 4889 (1983).

[3] R. Kubo, M. Toda, and N. Hashitsume, *Statistical Physics*, 2nd ed. (Springer-Verlag, Heidelberg, 1991).

[4] J. Cao and G. A. Voth, J. Chem. Phys. **100**, 5106 (1994).

[5] S. Jang and G. A. Voth, J. Chem. Phys. **111**, 2371 (1999).

[6] I. R. Craig and D. E. Manolopoulos, Journal of Chemical Physics **121** (8), 3368 (2004).

[7] D. R. Reichman, P. N. Roy, S. Jang, and G. A. Voth, Journal of Chemical Physics **113** (3), 919 (2000); E. Geva, Q. Shi, and G. A. Voth, Journal of Chemical Physics **115** (20), 9209 (2001); A. Horikoshi and K. Kinugawa, Journal of Chemical Physics **122** (17) (2005); I. R. Craig and D. E. Manolopoulos, Chemical Physics **322** (1-2), 236 (2006).

[8] W. H. Miller, J. Chem. Phys. **53**, 3578 (1970); W. H. Miller, Journal of Chemical Physics **95** (12), 9428 (1991); E. J. Heller, Journal of Chemical Physics **95** (12), 9431 (1991); E. J. Heller, Journal of Chemical Physics **94** (4), 2723 (1991); M. F. Herman and E. Kluk, Chem. Phys. **91**, 27 (1984); K. G. Kay, J. Chem. Phys. **100**, 4377 (1994); K. G. Kay, J. Chem. Phys. **100**, 4432 (1994).

[9] W. H. Miller, Journal of Physical Chemistry A **105** (13), 2942 (2001).

[10] H. B. Wang, X. Sun, and W. H. Miller, Journal of Chemical Physics **108** (23), 9726 (1998).

[11] X. Sun and W. H. Miller, Abstracts of Papers of the American Chemical Society **213**, 94 (1997).

[12] J. Liu and W. H. Miller, Journal of Chemical Physics **125** (22) (2006).

[13] H. W. Lee and M. O. Scully, Journal of Chemical Physics **73** (5), 2238 (1980).

[14] J. A. Poulsen, G. Nyman, and P. J. Rossky, J. Chem. Phys. **119**, 12179 (2003); Q. Shi and E. Geva, J. Phys. Chem. A **107**, 9059 (2003).

[15] J. Shao and N. Makri, J. Phys. Chem. A **103**, 7753 (1999).

[16] J. Shao and N. Makri, J. Phys. Chem. A **103**, 9479 (1999); N. J. Wright and N. Makri, J. Phys. Chem. B **108**, 6816 (2004); A. Nakayama and N. Makri, Chem. Phys. **304**, 147 (2004); J. Liu and N. Makri, Chemical Physics **322** (1-2), 23 (2006).

[17] J. Liu, A. Nakayama, and N. Makri, Molecular Physics **104** (8), 1267 (2006).

[18] W. H. Miller, Faraday Discussions (110), 1 (1998); X. Sun and W. H. Miller, Journal of Chemical Physics **110** (14), 6635 (1999); W. H. Miller, Journal of Chemical Physics **125** (13) (2006).

[19] E. Martin-Fierro and E. Pollak, Journal of Chemical Physics **125** (16) (2006).

[20] P. Frantsuzov, A. Neumaier, and V. A. Mandelshtam, Chemical Physics Letters **381** (1-2), 117 (2003); P. A. Frantsuzov and V. A. Mandelshtam, Journal of Chemical Physics **121** (19), 9247 (2004); J. S. Shao and E. Pollak, Journal of Chemical Physics **125** (13) (2006).

[21] E. P. Wigner, Phys. Rev. **40**, 749 (1932).

[22] M. Hillery, R. F. Oconnell, M. O. Scully, and E. P. Wigner, Physics Reports-Review Section of Physics Letters **106** (3), 121 (1984); K. Takahashi, Prog. Theor. Phys. Suppl. **98**, 109 (1989); H. W. Lee, Physics Reports-Review Section of Physics Letters **259** (3), 147 (1995).

[23] H. W. Lee and M. O. Scully, Journal of Chemical Physics **77** (9), 4604 (1982).

[24] A. Donoso and C. C. Martens, Physical Review Letters **8722** (22), art. no. (2001).

[25] J. Liu and N. Makri, Journal of Physical Chemistry A **108** (25), 5408 (2004); J. Liu and N. Makri, Molecular Physics **103** (6-8), 1083 (2005).

[26] Q. Shi and E. Geva, J. Phys. Chem. A **107** (9070-9078) (2003); J. A. Poulsen, G. Nyman, and P. J. Rossky, Journal of Physical Chemistry B **108** (51), 19799 (2004).

[27] E. Jezek and N. Makri, J. Phys. Chem. **105**, 2851 (2001); M. Thoss, H. B. Wang, and W. H. Miller, Journal of Chemical Physics **114** (21), 9220 (2001); N. J. Wright and N. Makri, Journal of Chemical Physics **119** (3), 1634 (2003).

[28] W. H. Zurek, Nature **412** (6848), 712 (2001); T. Dittrich, C. Viviescas, and L. Sandoval, Physical Review Letters **96** (7) (2006).

[29] E. J. Heller, J. Chem. Phys. **65**, 1289 (1976).

[30] N. Makri and K. Thompson, Chem. Phys. Lett. **291**, 101 (1998); K. Thompson and N. Makri, Physical Review E **59** (5), R4729 (1999).

[31] K. Husimi, Prog. Phys. Math. Soc. Japan **22**, 264 (1940).

[32] R. J. Glauber, Physical Review **131** (6), 2766 (1963); R. J. Glauber, *Quantum Optics and Electronics* (Gordon and Breach, New York, 1965); E. C. G. Sudarshan, Physical Review Letters **10** (7), 277 (1963).

[33] H. C. Andersen, Journal of Chemical Physics **72** (4), 2384 (1980).

[34] S. Nose, Journal of Chemical Physics **81** (1), 511 (1984); W. G. Hoover, Physical Review A **31** (3), 1695 (1985).

Figure Captions

Fig. 1 (Color online). The symmetrized force autocorrelation function for the one-dimensional anharmonic oscillator given in Eq. (5.1) for $\beta = 1$. Black solid line: Exact quantum result. Cyan dotted line: Classical result. In the following results, the Boltzmann operator is treated by the TGA. Purple dot-dashed line: LSC-IVR result. Green solid circle: Full WD result. Red triangle: Full DMD result. Brown dashed line: 2^{nd} order WD result. Blue solid line: 2^{nd} order DMD result.

Fig. 2 (Color online). The real part of the standard momentum autocorrelation function for the one-dimensional anharmonic oscillator given in Eq. (5.1) for $\beta = 1$. Black solid line: Exact quantum result. Cyan dotted line: Classical result. In the following results, the Boltzmann operator is treated by the TGA. Purple dot-dashed line: LSC-IVR result. Green solid circle: Full WD result. Red triangle: Full DMD result. Brown dashed line: 2^{nd} order WD result. Blue solid line: 2^{nd} order DMD result.

Fig. 3 (Color online). As in Fig. 1, but for a much lower temperature $\beta = 8$. Panel (b) and (c) show a blowup of the curves shown in (a).

Fig. 4 (Color online). As in Fig. 2, but for a much lower temperature $\beta = 8$.

Fig. 5 (Color online). The symmetrized force autocorrelation function for the one-dimensional quartic potential given in Eq. (5.2) for $\beta = 1$. Black solid line: Exact quantum result. Cyan dotted line: Classical result. In the following results, the Boltzmann operator is treated by the TGA. Purple dot-dashed line: LSC-IVR result. Green solid circle: Full WD result. Red triangle: Full DMD result. Brown dashed line: 2^{nd} order WD result. Blue solid line: 2^{nd} order DMD result.

Fig. 6 (Color online). The real part of the standard momentum autocorrelation function for the one-dimensional quartic potential given in Eq. (5.2) for $\beta = 1$. Black solid line: Exact quantum result. Cyan dotted line: Classical result. In the following results, the Boltzmann operator is treated by the TGA. Purple dot-dashed line: LSC-IVR result. Green solid circle: Full WD result. Red triangle: Full DMD result. Brown dashed line: 2^{nd} order WD result. Blue solid line: 2^{nd} order DMD result.

Fig. 7 (Color online). As in Fig. 5, but for a much lower temperature $\beta = 8$. Panel (b) and (c) show a blowup of the curves shown in (a).

Fig. 8 (Color online). As in Fig. 6, but for a much lower temperature $\beta = 8$.

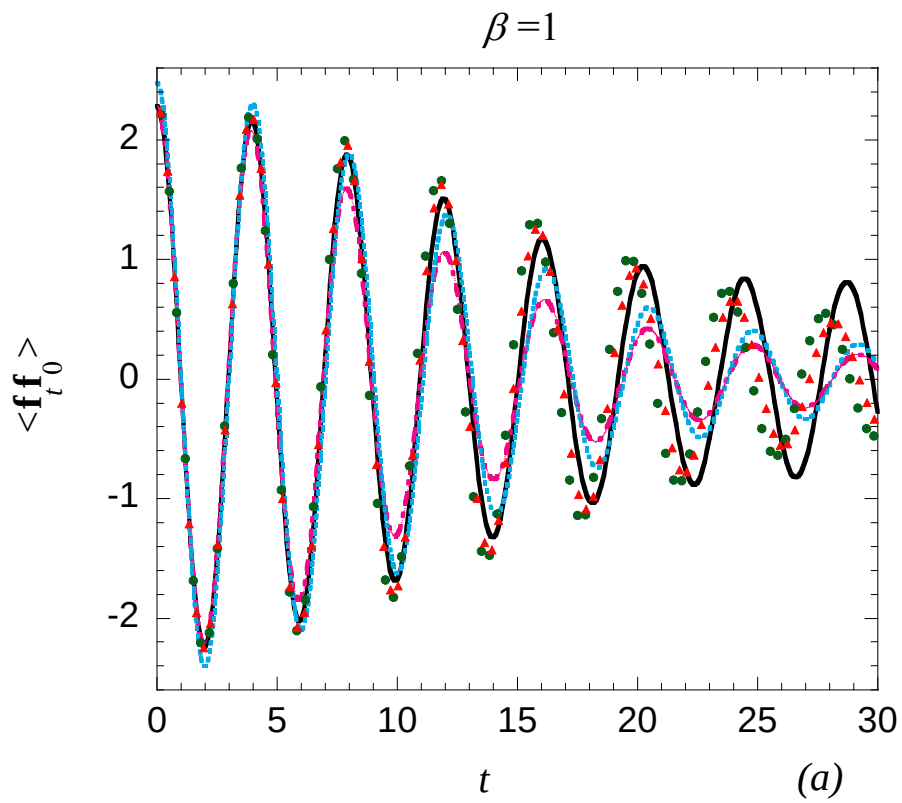
β =1
<f f>t 0
2
1
0
-1
-2
0
5
10
15
20
25
30
t
(a)

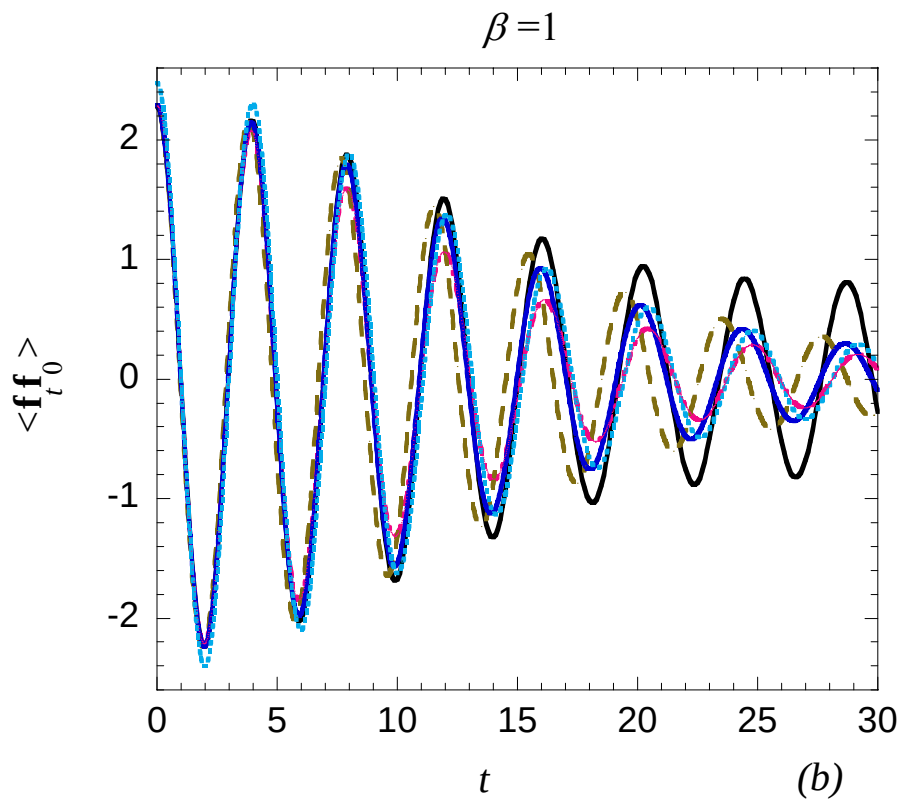
β =1
<f f>t 0
2
1
0
-1
-2
0
5
10
15
20
25
30
t
(b)

Fig. 1

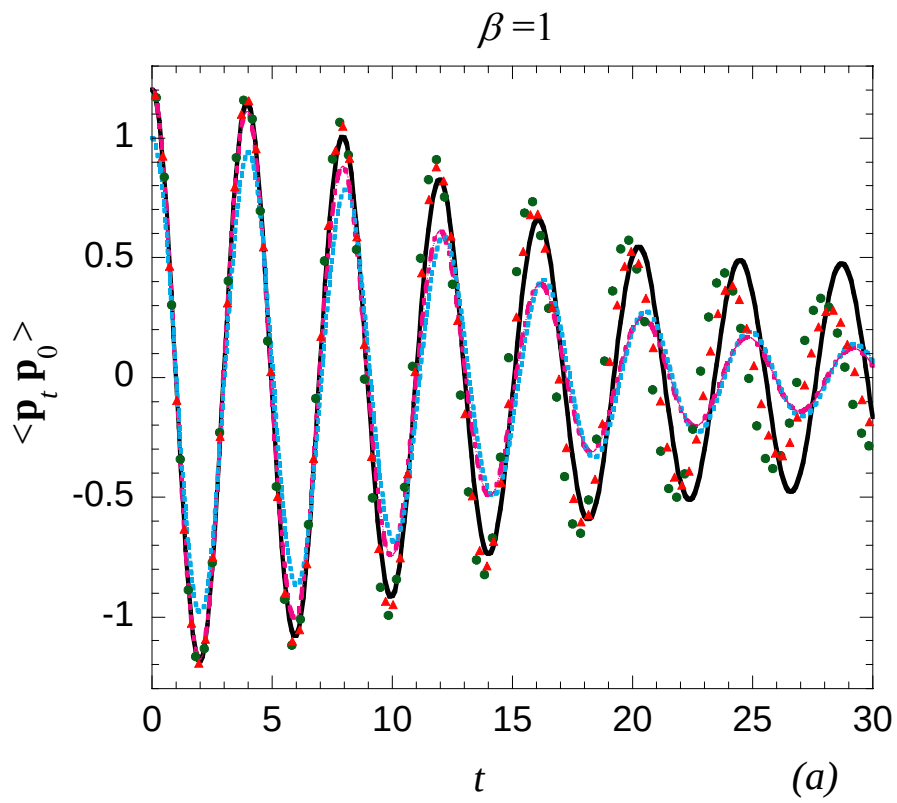
β =1
<p_t p_0>
1
0.5
0
-0.5
-1
0
5
10
15
20
25
30
t
(a)

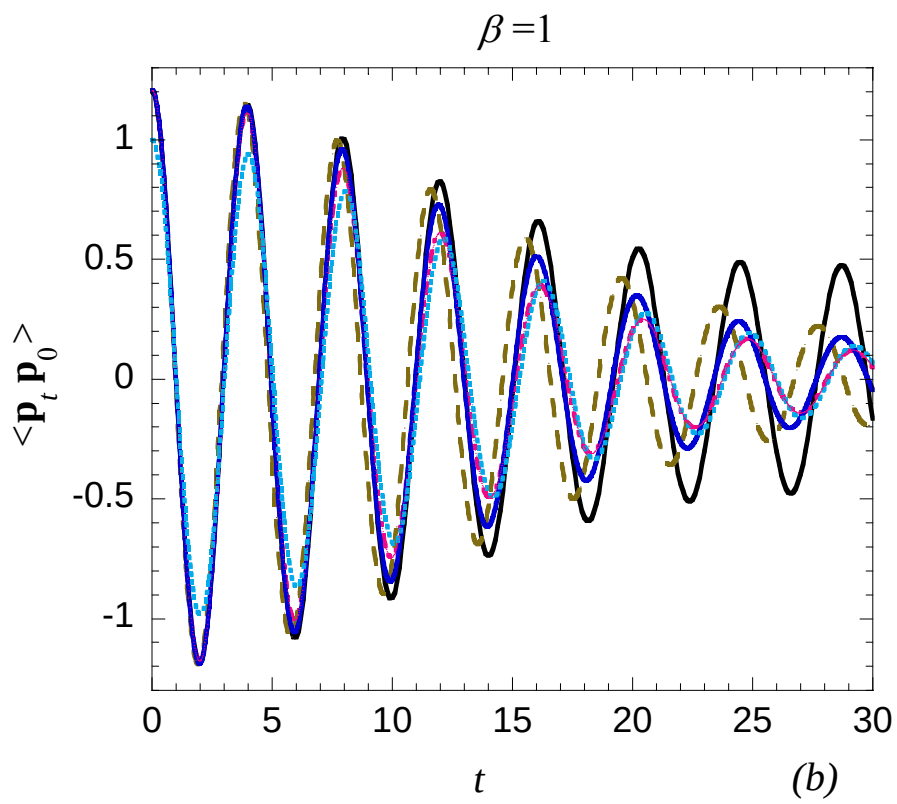
β =1
<p_t p_0>
1
0.5
0
-0.5
-1
0
5
10
15
20
25
30
t
(b)

Fig. 2

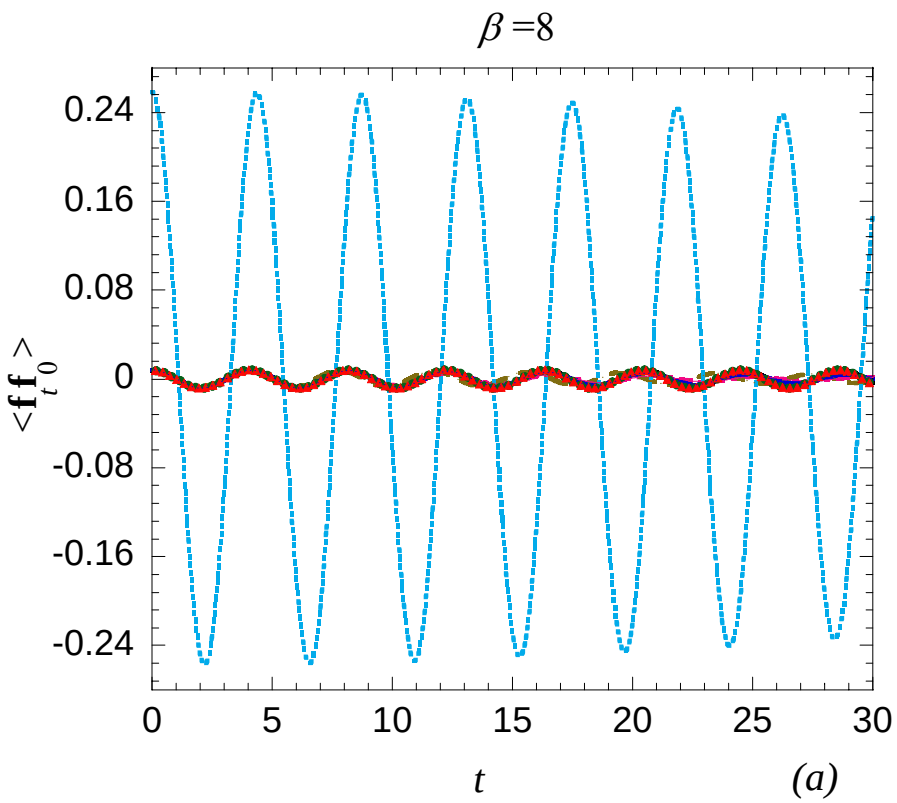
β =8
0.24
0.16
0.08
0
-0.08
-0.16
-0.24
<f f>t 0
0
5
10
15
20
25
30
t
(a)

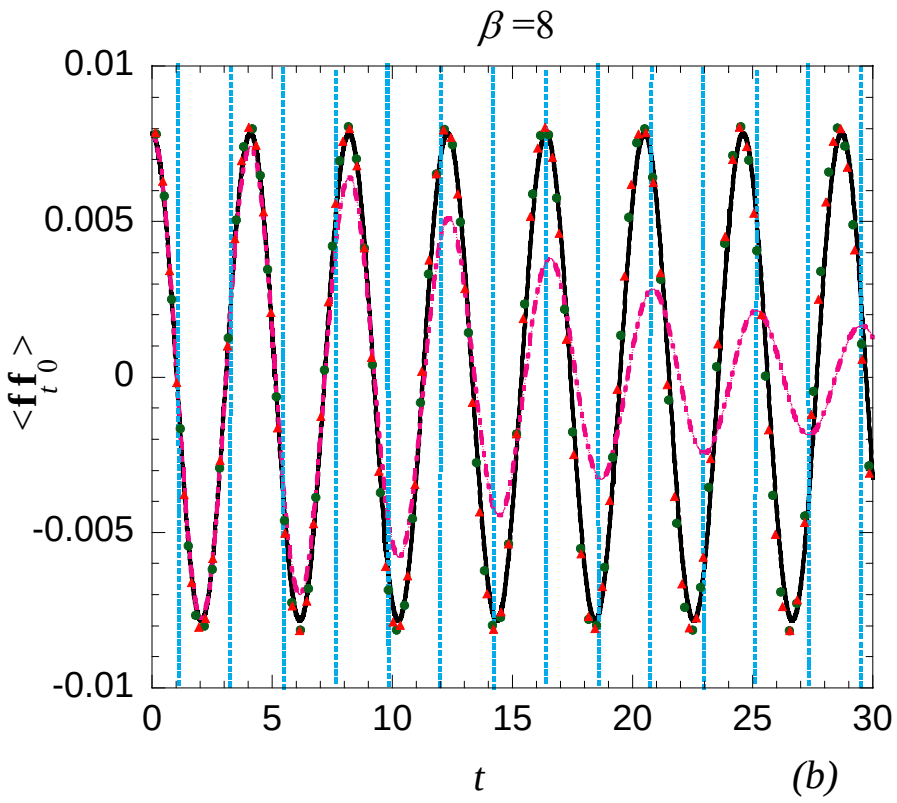
β =8
0.01
0.005
0
-0.005
-0.01
<f f>t 0
0
5
10
15
20
25
30
t
(b)

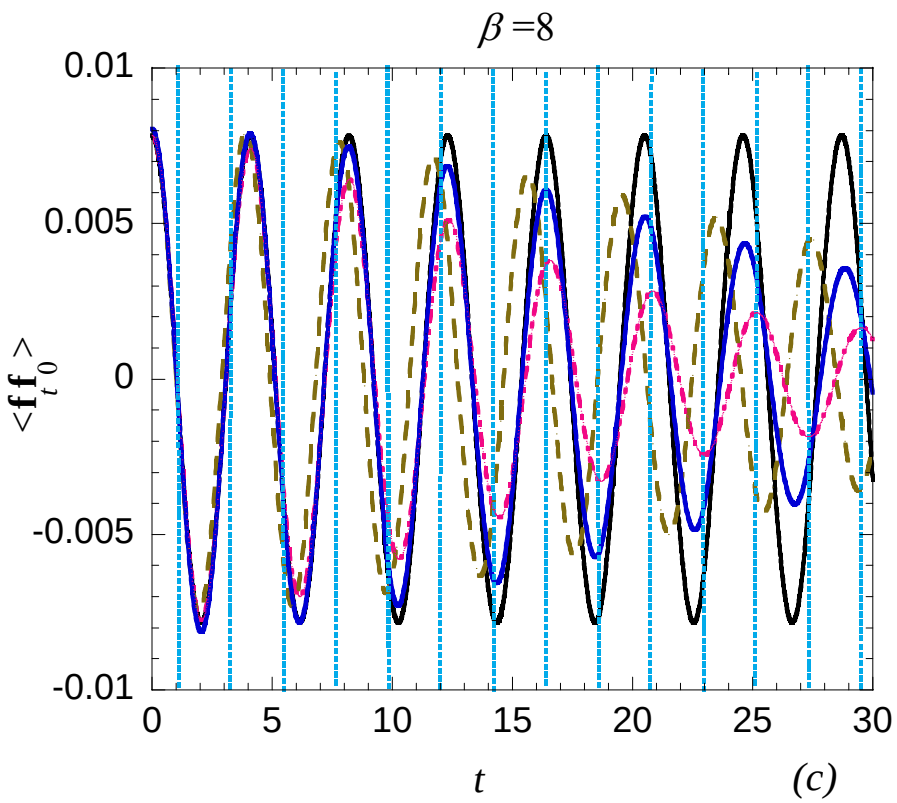

Fig. 3

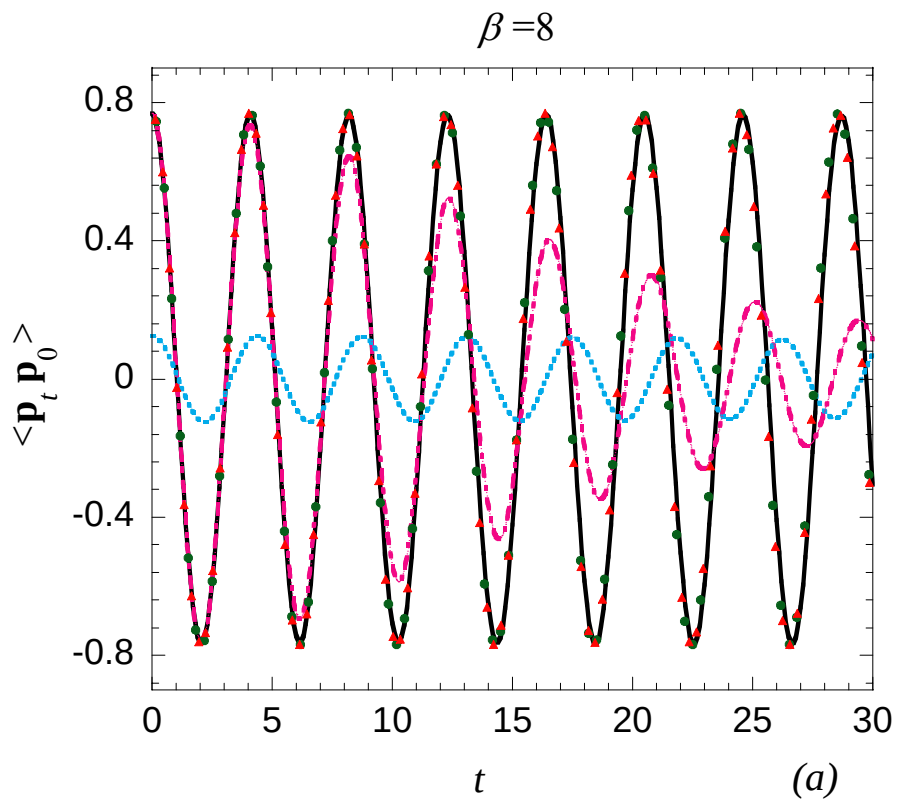
β =8
0.8
0.4
0
-0.4
-0.8
0
5
10
15
20
25
30
t
(a)

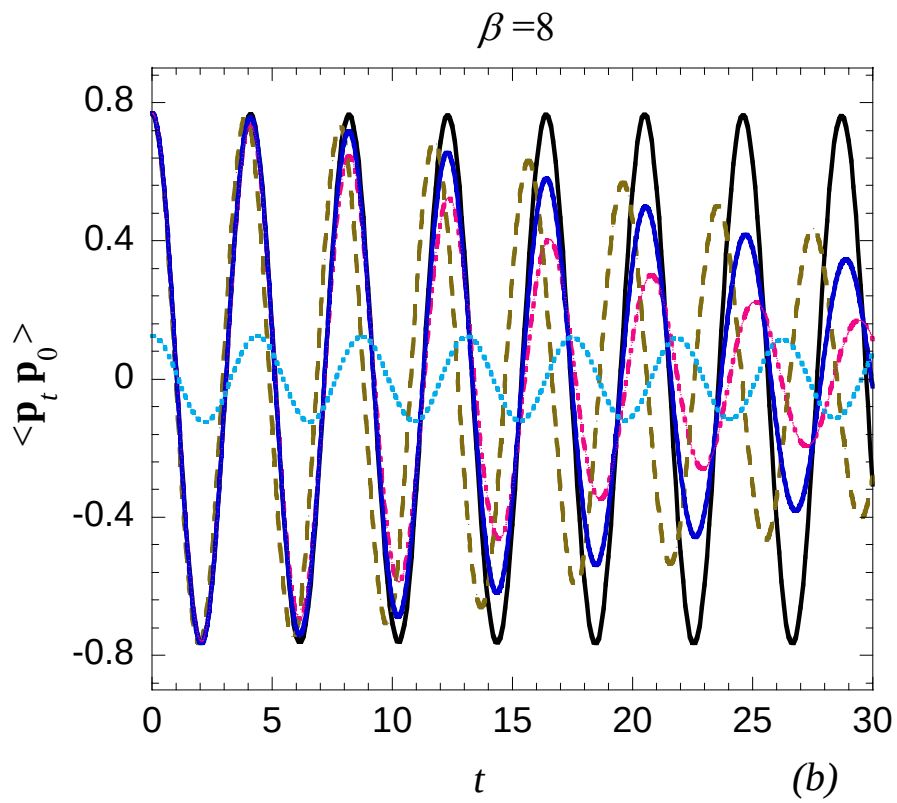
β =8
0.8
0.4
0
-0.4
-0.8
0
5
10
15
20
25
30
t
(b)

Fig. 4

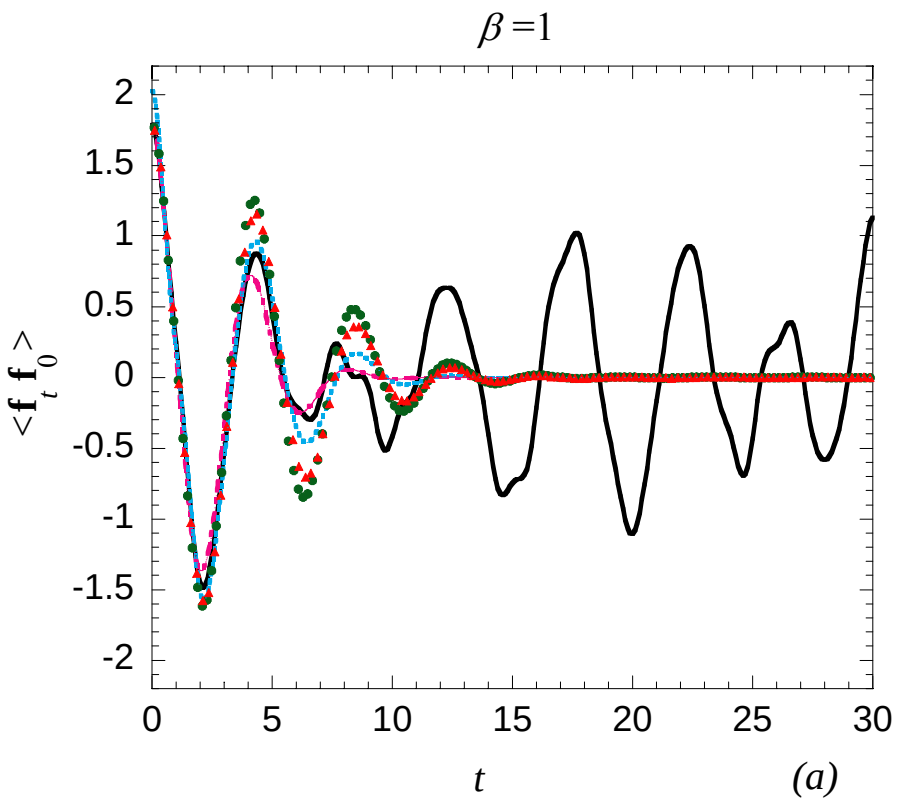

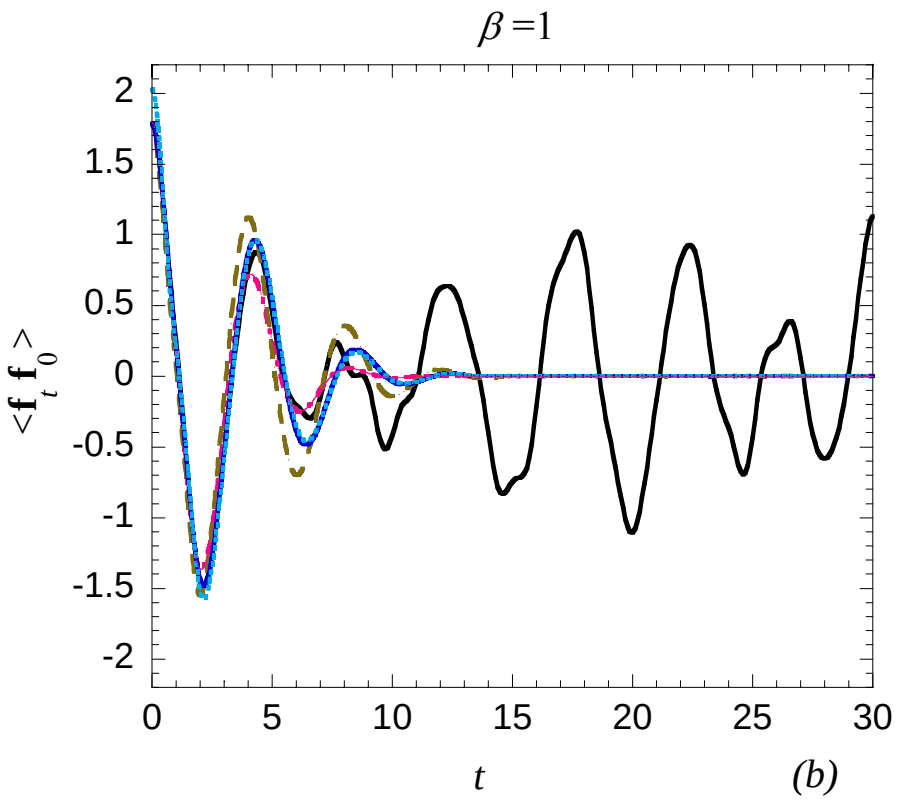

Fig. 5

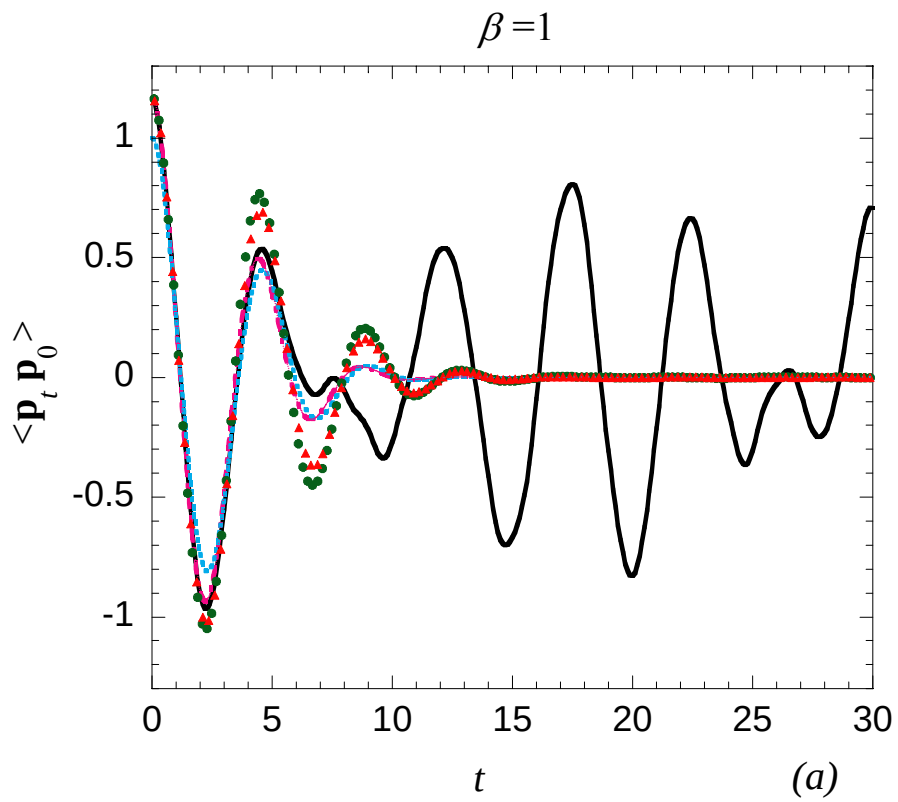
β =1
<p_t p_0>
1
0.5
0
-0.5
-1
0
5
10
15
20
25
30
t
(a)

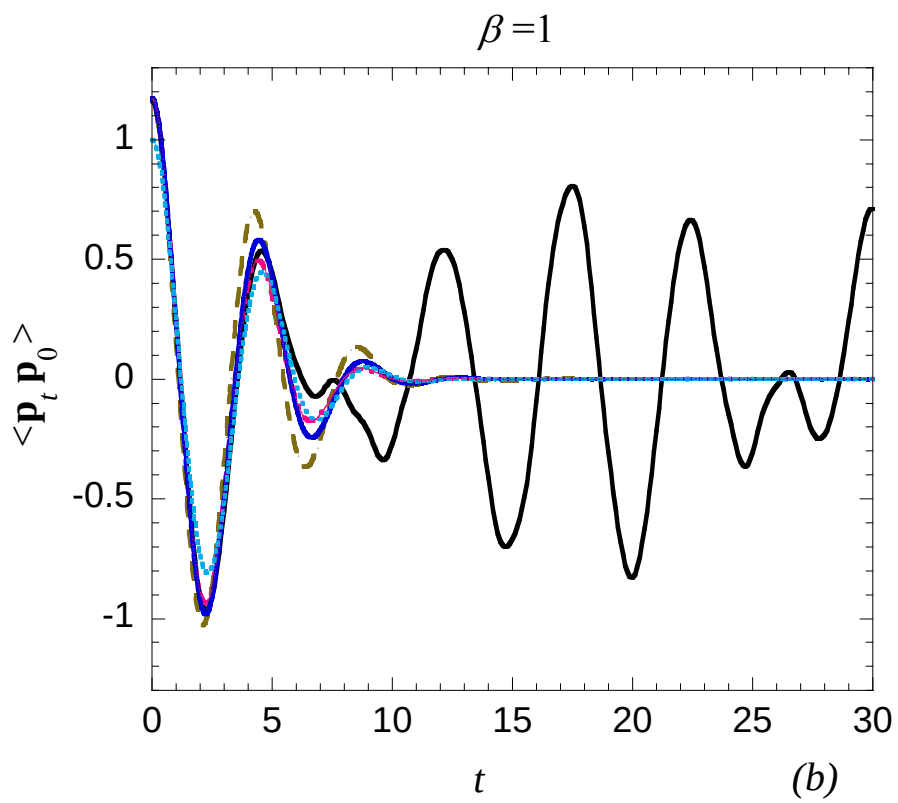
β =1
<p_t p_0>
1
0.5
0
-0.5
-1
0
5
10
15
20
25
30
t
(b)

Fig. 6

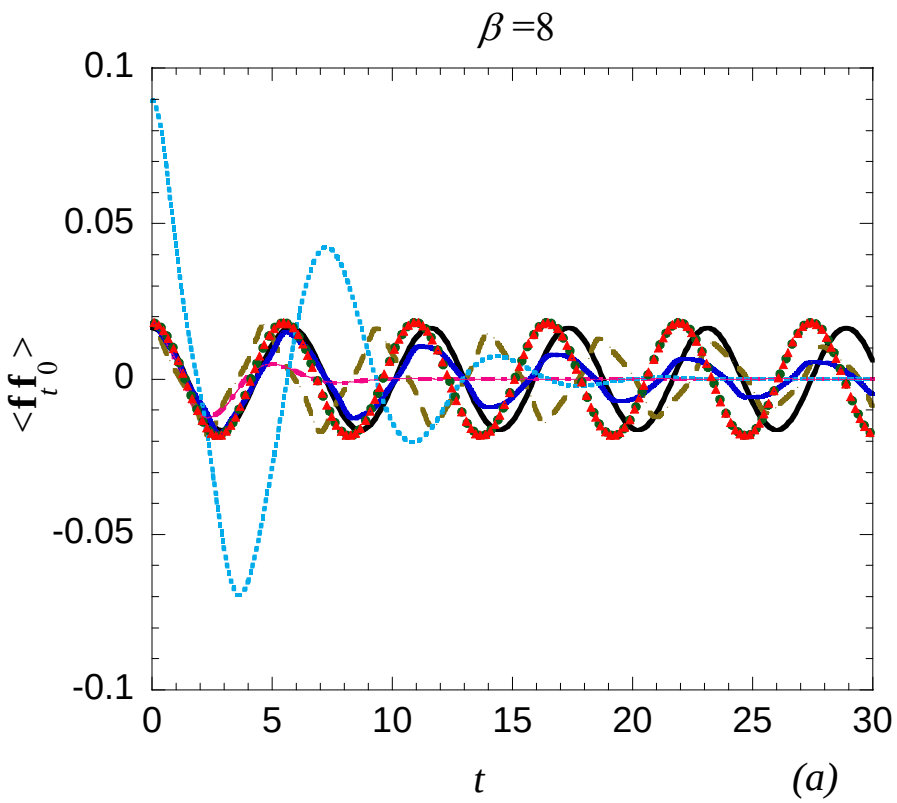
β =8
0.1
0.05
0
-0.05
-0.1
0
5
10
15
20
25
30
t
(a)

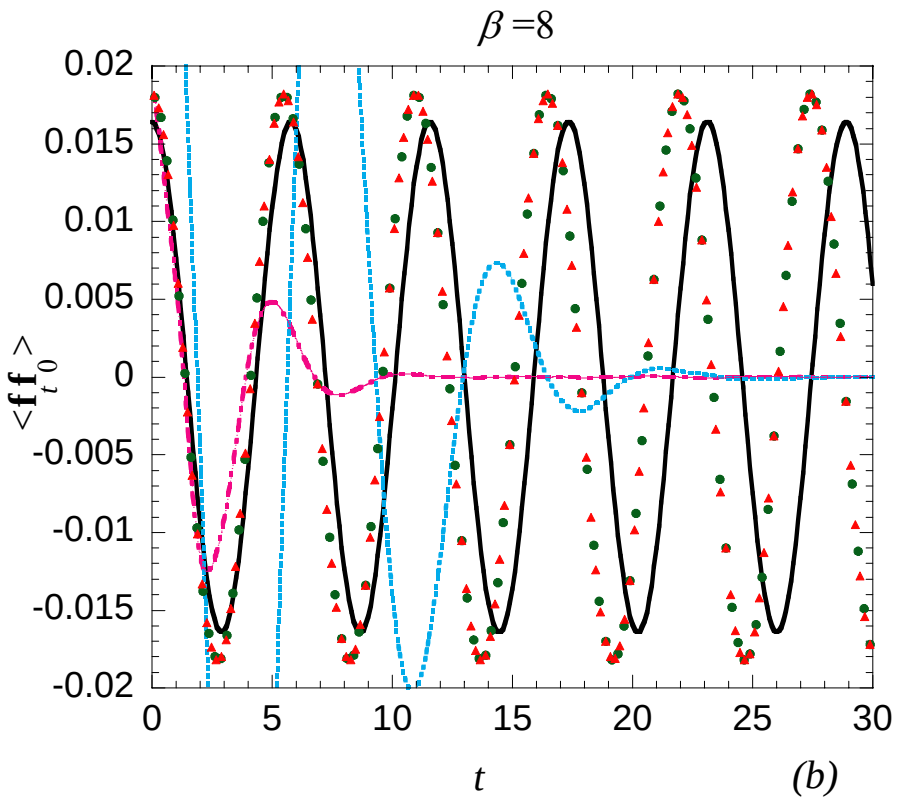
β =8
0.02
0.015
0.01
0.005
0
-0.005
-0.01
-0.015
-0.02
0
5
10
15
20
25
30
t
(b)

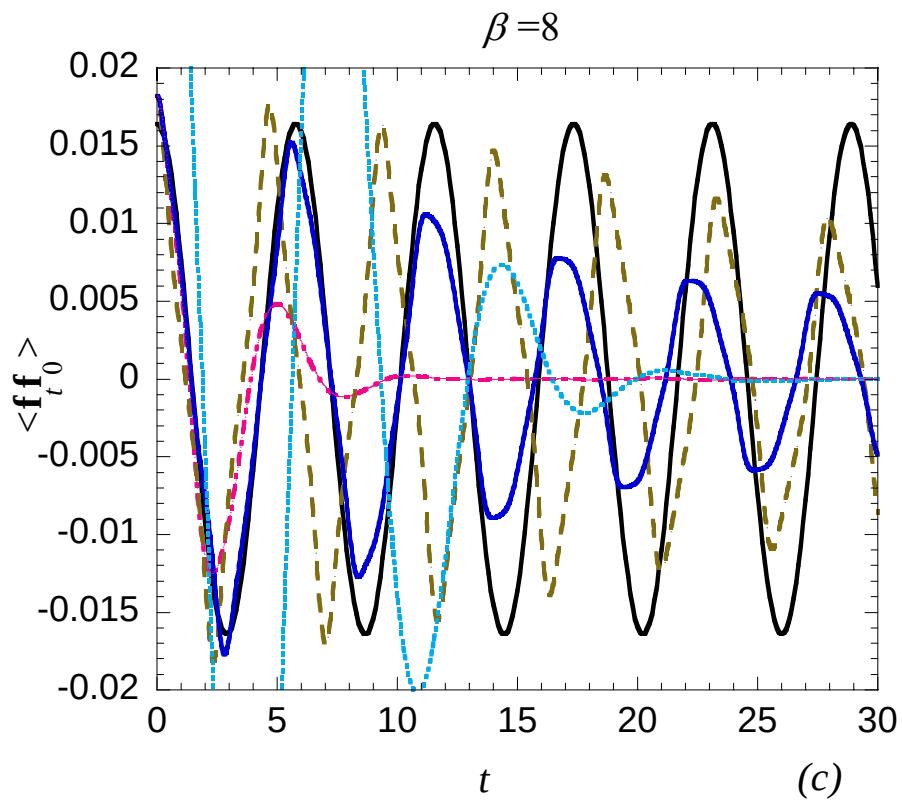

Fig. 7

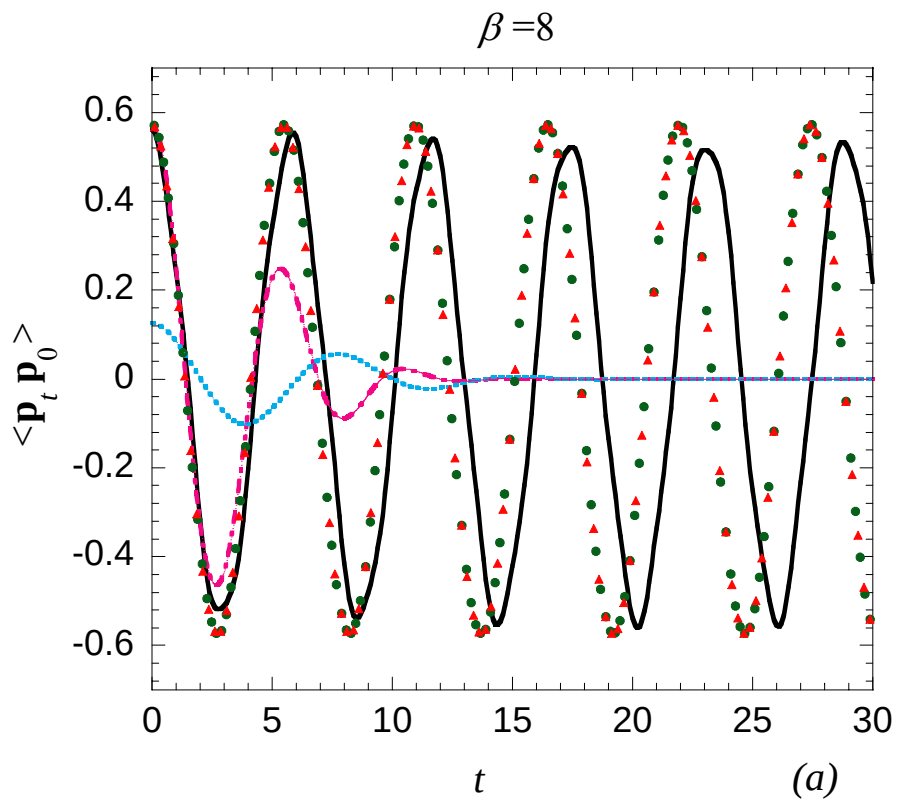
β =8
0.6
0.4
0.2
0
-0.2
-0.4
-0.6
0
5
10
15
20
25
30
t
(a)

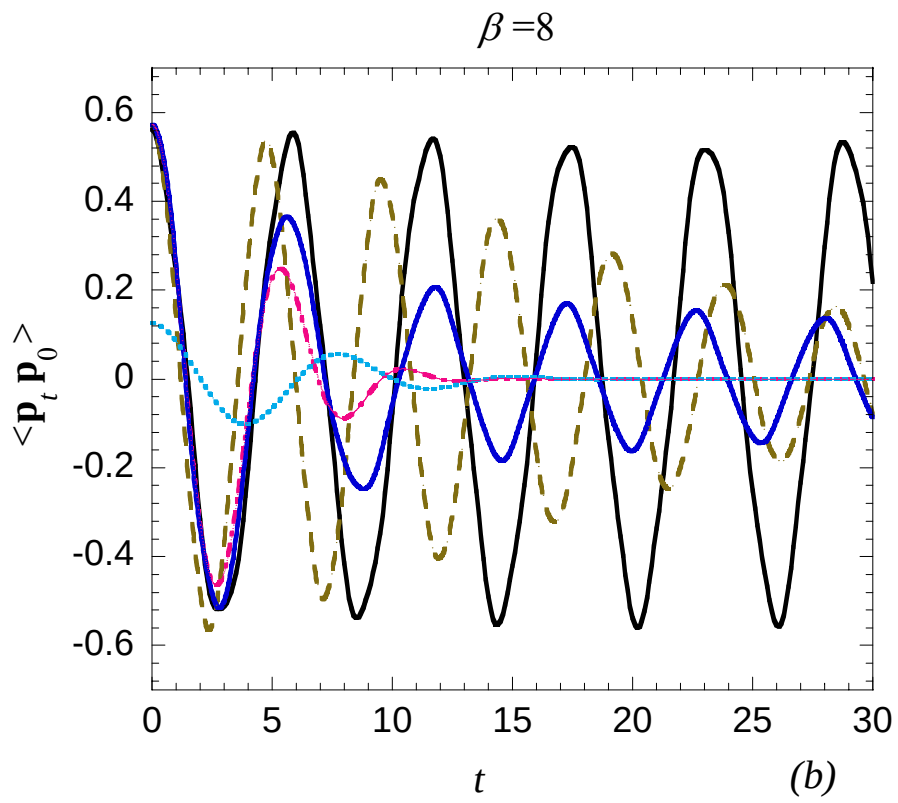
β =8
0.6
0.4
0.2
0
-0.2
-0.4
-0.6
0
5
10
15
20
25
30
t
(b)

Fig. 8